All-in-one: A spectral imaging laboratory system for standardised automated image acquisition and real-time spectral model deployment
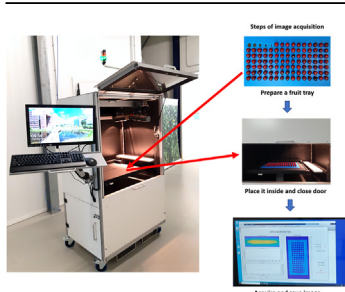
Puneet Mishra [*], Menno Sytsma , Aneesh Chauhan , Gerrit Polder , Erik Pekkeriet

Agro-Food Robotics, Wageningen University & Research, the Netherlands

HIGHLIGHTS

- A fully integrated spectral imaging system is presented.
- The system allows real-time data acquisition and model deployment.
- The system was tested for predicting fruit properties.
- The system allows a non-expert approach to spectral imaging.

GRAPHICAL ABSTRACT

ABSTRACT

Spectral imaging (SI) in analytical chemistry is widely used for the assessment of spatially distributed physicochemical properties of samples. Although massive development in instrument and chemometrics modelling has taken place in the recent years, the main challenge with SI is that available sensors require extensive system integration and calibration modelling before their use for routine analysis. Further, the models developed during one experiment are rarely useful once the system is reintegrated for a new experiment. To avoid system reintegration and reuse calibrated models, this study presents an intelligent All-In-One SI (ASI) laboratory system allowing standardised automated data acquisition and real-time spectral model deployment. The ASI system supplies a controlled standardised illumination environment, an in-built computing system, embedded software for automated image acquisition, and model deployment to predict the spatial distribution of sample properties in real-time. To show the capability of the ASI framework, exemplary cases of fruit property prediction in different fruits are presented. Furthermore, ASI is also benchmarked in performance against the current commercially available portable as well as high-end laboratory spectrometers.

© 2021 The Author(s). Published by Elsevier B.V. This is an open access article under the CC BY license (http://creativecommons.org/licenses/by/4.0/).

1. Introduction

Optical spectroscopy is the study of the interaction of electromagnetic radiation (EMR) with the matter. Typically, when the matter is illuminated with EMR three major optical phenomena occur, reflection, transmission, and absorption. The extent of the dominance of the phenomenon depends on the physicochemical properties of matter. Since optical spectroscopy allows non-destructive and non-contact analysis of the matter, its applications are prevalent in various domains such as food, medical,

* Corresponding author.;
E-mail addresses: puneet.mishra@wur.nl, shiva.mishra2@gmail.com (P. Mishra).

pharmaceutical, and many more, that require non-invasive assessment of physicochemical properties of samples matrices [1–4].

Although optical spectroscopy can be performed over a wide range of EMR, the most frequently and routinely used technique for non-destructive prediction of physicochemical properties is based on the visible (Vis) and near-infrared (NIR) range of EMR i.e. 350-2500 nm [5]. The interaction of Vis-NIR light with the samples results in two main optical phenomena i.e., absorption and scattering, where scattering is the result of the interaction of light with the physical properties of samples, while the absorption is due to the presence of chemical components having OH, NH and CH bonds in the samples [6,7]. Due to the presence of both scatter and absorption, the optical spectroscopy in the Vis-NIR range can be used for the prediction of simple colour pigments, macromolecules such as proteins, fats, moisture and sugar, as well physical properties such as particle size, texture [5].

In recent decades, significant developments in the domain of optical spectroscopy have taken place. The main development from the perspective of rapid samples analysis is the availability of portable low-cost spectral sensors (both point as well as imaging) which allows easy measurement of spectral signals from samples in either reflection or interaction mode [8–10]. The main benefit of portable spectral sensors is that they allow the sensor to be carried to the samples when the samples cannot be brought to the sensor [9]. A key factor in the implementation of Vis-NIR spectroscopy is the sensor calibration and model development which is dependent on the chemometric analysis of data [7,11]. Almost all spectral sensors require calibration and model development, unless models from a similar instrument are available. In the latter case, the models can be transferred between instruments using advanced calibration transfer techniques [11,12]. Major developments have also taken place in the domain of chemometric data analysis such as the development of ensemble modelling approaches [13] as well as the combination of chemometrics and deep learning [14–17] which have outperformed classical chemometric approaches used for traditional modelling of spectral data.

For Vis-NIR spectroscopy, sensors for both the point measurement [18,19] as well as the imaging spectroscopy [20–22] modality, called spectral imaging (SI), are available in the market. The main difference between the point spectrometer and SI is that the point spectrometer only allows measuring a single spot on the sample, while the SI measures the complete sample in a single scan where each pixel are the spectra from the imaged scene [21]. Hence, SI allows exploring spatially resolved spectral properties of samples [23]. The point spectroscopy-based sensors are usually portable and even pocket-sized [9], while the SI sensors are bigger in size and are more suitable for cases requiring high-throughput analysis. SI is essential whenever the analysis requires assessment of the spatial distribution of sample properties or detection of any localised anomaly on samples' surface which is difficult to access with a point measurement [24,25].

Although plentiful applications of Vis-NIR SI can be found in the scientific literature [18,19,26–28], when it comes to the practical implementation of the technique for routine analysis, the number is difficult to access. A major reason for it is because most of the SI sensors in the market are currently supplied as data acquisition tools, and the user needs to design experimental setups where the sensor needs to be integrated into a well calibrated measurement setup, before any measurement can be done, and models developed. Moreover, the best practice followed in research laboratories is usually to perform the sensor operation/spectral data acquisition and data modelling in separate steps. Although this approach has shown promising potential and has resulted in plentiful research [18,19], it cannot be considered a practical solution for routine use

by non-experts. In the domain of point spectroscopy, this concern is now addressed, and several spectrometer manufacturers now offer spectrometers with embedded computing where the models can be deployed and used for real-time prediction of sample properties [18,19]. The portable spectrometer manufacturers are also supplying the instruments pre-loaded with models which users can directly apply without any need to recalibrate the instrument from scratch [5,9].

Even though major developments can be seen in the development of embedded portable point spectroscopy, the development of SI as a routine tool is still lacking, making the technology inaccessible for non-expert users. One of the primary challenges with SI is that market available cameras require extensive system integration and calibration modelling before any experiment can be performed. Further, the models developed during one experiment are rarely useful once the system is reintegrated for a new experiment. To avoid system reintegration and reuse of calibrated models for practical use, the best approach is to develop a standardised SI system with embedded computing to have minimal influence from unwanted sources on the measurement. In the current state of the art laboratory use, SI can be majorly divided into two steps: the first step is to use the software supplied by the camera manufacturer for data acquisition, and the second step is data analysis using either open source [29] or commercial SI processing software. Such an approach facilitates laboratory research but is not a practical solution for routine analysis by non-expert users such as lab technicians. In a practical scenario, one can assume a standardised SI system with pre-loaded models to be an ideal solution as it allows repeatable measurement, with minimal effort, from a non-expert user in terms of system use and management.

The aim of this study was to develop an intelligent all-in-one spectral imaging (ASI) laboratory system for standardised automated data acquisition and real-time spectral model deployment. The ASI system supplies a controlled standardised illumination environment, an in-built computing system, embedded software for automated image acquisition and model deployment to predict the spatial distribution of sample properties in real-time. The automation covered two main parts: first, the mechanical automation based on the integration of the line-scan SI camera and lightning with a linear stage inside a closed blackout cabinet; the second part relates to the development of software tools for simultaneous control of the camera and linear stage for data acquisition and simultaneous deployment of the pre-loaded models for the prediction of spatially distributed sample properties. To show the capability of the ASI framework, exemplary cases of fruit property prediction in several fruits were conducted. Key novelties related to the development of the ASI are as follow:

- This is the first setup that brings the concept of embedded spectral imaging to life for non-expert users as well as the analytical chemistry community.
- In the ever-growing era of sensing and data, just like the development of new fundamental analytical chemistry techniques, it is especially important to automate the analytical sensing techniques for their widespread use and reuse of data which are generated in experiments.
- Currently, in most scientific studies related to SI, the concept of data and models reuse is rarely practiced. ASI brings forward an integrated setup for fair and sustainable usage of data and models generated in novel experiments.
- Although several of the camera manufacturers supply basic software for data acquisition or for modelling, there is no single solution that is capable of controlling cameras, translation stage, automated referencing, automated image acquisition, model

deployment. The embedded software tool with these capabilities is another key contribution.

- The last novelty of the ASI is the push-button approach to SI. One of the main contributions of the work is the simplification of the usage of the analytical technique (in this study spectral imaging). This will allow any non-expert users of spectral imaging in the analytical chemistry community technique to use and explore the technique.

2. Materials and method

2.1. All-in-one spectral imaging setup

The ASI setup was designed as a closed system. The system was designed as a closed form to keep the illumination standardised and to avoid any influence caused by external light in the operating room. One of the aims while designing the ASI setup was to have a portable setup that can be easily carried to various locations based on the experimental needs. To keep the system portable, the ASI setup was mounted on four wheels. An image of the ASI setup is shown in Fig. 1. Apart from the physical setup there were four main electronic components in the system: a line-scan hyperspectral camera and halogen lights; a linear stage where the line-scan camera and the lights were mounted; an automated height adjustment platform for samples presentation; and a computer system which connects with the camera and the linear stage. The

setup uses the FX10 Vis-NIR spectral camera (Specim, Oulu, Finland) which works in the spectral range of 400−1000 nm. These cameras have a high spatial resolution of 1024 pixels and 224 spectral bands. The FX10 camera was a gigabyte ethernet camera and connected to the main computer system over the ethernet port. A lens with a view angle of 38°, as supplied by the camera manufacturer, was used. In the current research, the lens with a view angle of 38° was sufficient due to the small size of the fruit crate, however, based on the necessity the user can buy different lenses from the camera manufacturer and improve their system. Since the camera was a line scan, it was mounted on a servomotor-actuated spindle axis from Festo (Esslingen, Germany). This linear stage was controlled with a CMMT-AS servo drive, also from Festo. The servo drive communicated with the computer system via Ethernet and ran with the MODBUS TCP/IP protocol using the software drivers supplied by the drive manufacturer. The Festo servo drive was first commissioned with the Festo automation suite and later controlled with the in-house software. The commissioning of servo drive is an essential step to synchronize different electronic components of the complete system. Along with the camera, the halogen lamps were also mounted on the linear stage on side of the camera to supply homogenous illumination in the field of view of line scan. Two halogen lamps, with 3 halogen bulbs each, were integrated sidewise to the camera. The halogen lamps were supplied by the camera manufacturer (Specim, Oulu, Finland). The linear stage, the camera, and the light source are mounted at the top with a view to nadir. The cabinet has a push-button height adjustment platform
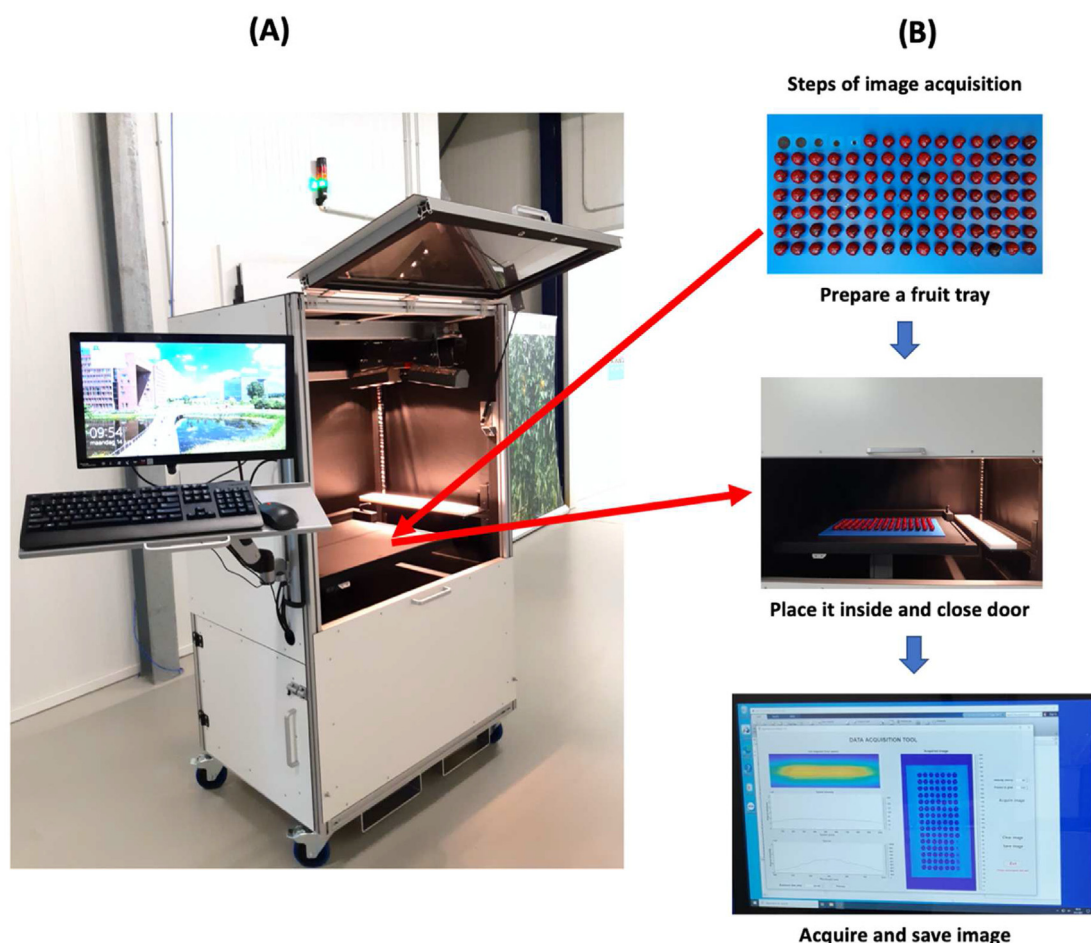

Fig. 1. An overview of the All-In-One spectral imaging (ASI) setup. (A) The ASI setup, and (B) workflow of ASI setup for spectral imaging.

that can be electronically controlled to increase or decrease the distance of the samples from the camera. Automated height adjustment allows a wide variety of samples to be measured with the setup i.e., from grapes to melons. The setup is provided with a periphery touchscreen (Illyama, Nagona, Japan) which allows the setup control of multiple tasks such as data acquisition, model deployment and visualisation. The setup is also provided with a periphery keyboard and a mouse (Logitech, Lausanne, Switzerland) if the user intends to control the system without interacting with the touchscreen.

2.2. Software for real time acquisition and model deployment

2.2.1. Data acquisition

The software in the setup is an essential part of the ASI. Some commercial software such as Prediktera (https://prediktera.com/), Perception parks (https://www.perception-park.com/perception-park) and perClass Mira (https://www.perclass.com/apps/perclass-mira) are emerging in the market, but their applicability is application centric, and users have limited freedom to control different mechanical components, explore the data and implementation of optimized model. Therefore, to advance the application of HSI, we herein designed and developed a user-friendly software interface for controlling the actuation of the mechanical components, image collection and real-time data analysis and result visualisation which if required, can further be adopted for different applications, and thus accelerate the speed of quality analysis tests in both laboratory and industrial environment which is not possible with existing commercial software. It is also the first software in the chemometric community that allows real-time data acquisition and model deployment. The developed software can be divided into two parts, the first part deals with communication and operation of the camera and the linear stage for data acquisition, and the second part allows handling the acquired data by performing radiometric calibration and later model deployment. The software also allows visualisation of the predicted traits. The software is based on MATLAB 2018b and developed as an independent standalone application. For camera connection with the GigE interface, the software uses the GigE vision toolbox from MathWorks, USA (United States of America). The GigE interface allows loading the camera as an object as well as several pre-available functions to preview the output of the camera in real-time. The settings of the camera, such as exposure time, frame rate, spatial and spectral binning, can be changed by assigning the property value to the camera object. The preview tool can be used to visualise the real-time output from the camera which allows real-time adjustment of the exposure time best suited for the application. The setup also has an integrated white Teflon plate used as a white reference for radiometric correction of the images. The white Teflon plate is scanned before any imaging and all images are independently radiometrically corrected to drop any differences due to illumination intensity fluctuations in the reflection measurements. The dark current is also measured prior to any imaging by automatically closing the shutter of the camera. The image frames were acquired using the 'snapshot' function from the GigE vision toolbox implemented inside a loop. The linear stage was also controlled from the MATLAB app using software drivers provided by Festo, Germany along with the servo drive. Since in the standardised setup the linear stage has the same motion and same travel distance, the only parameter requiring synchronisation with the camera frame capture was the travel speed of the linear stage. The travel speed was further optimized with the camera frame using a checker box plate in the FOV (field of view) of the camera. A best travel speed of 30 mm/s with a camera exposure time of 20 ms was provided as a default setting to the setup, although if the user

changes the height of the white reference plate, the user can use the checker box plate to reach the best travel speed by observing the pattern of the plate. After the controlled acquisition of the images, the software automatically performs the dark and the white reference correction to estimate the reflection as Eq. (1).

$$Reflectance = \frac{I - D}{W - D} \tag{1}$$

where I is the radiance of the captured FOV, D is the dark current of the sensors and W is the radiance measured for the white reference. A point to note is that the software, together with automated image acquisition in the ASI setup, by default provides the reflectance data which can be directly used for either modelling or model deployment.

2.2.2. Real-time model deployment and software output

A key feature of the ASI is that it allows real-time deployment of the models for predicting the property of interest. Once the reflectance data is collected, the samples of interest can be segmented from the background, for example, for fresh produce, such as fruit and plants, using a threshold (>0.3 for fruit) on the normalised difference vegetation index (NDVI). NDVI was used as it attains high value for fresh produce (~1) and can easily segment the fruit from the background scene consisting of non-fresh produce. After the segmentation, the pre-calibrated partial least-square regression (PLSR) models based on the type of sample under study were automatically applied to each pixel representing the sample. The models used for predicting the properties were pre-calibrated PLSR models integrated into the software of the system. Although currently the ASI system only has models related to fruit property prediction, the list of models can be expanded depending on the need.

As the output, the user gets a property map which is an image presenting spatially distributed properties of the samples. To make the visualisation more interactive, the software can be adapted to identify automatically each individual sample in the imaged scene and generates bounding boxes around it and highlights the mean values of the predicted property. The software can also be easily adapted to integrate option to save the results with a push-button which exports the predicted properties as an excel file and the spatial maps of predicted properties as an image file. The user interface for the system is specifically designed by keeping non-expert users in mind and is operated using a simple touch screen interface.

2.3. Samples for demo analysis

To demonstrate the functionality of the ASI system, demonstrative analyses were carried out for predicting a key fruit property, soluble solids content (SSC), on multiple kinds of fruits. The SSC was chosen as the quality parameter as it is widely used in the fruit industry to assess the quality of fresh fruit and is related to the sweetness of the fruit. The 4 fruit cases, as used for the demonstration of ASI, are shown in Table 1.

All fruits were obtained from the local supermarket called Albert Heijn, Ede, The Netherlands. Before any experiment, all fruits were stabilised to the room temperature of ~22 °C to avoid any effects related to temperature differences. SSC of the extracted fruit juice was determined using a handheld refractometer (HI 96801, Hanna Instruments Inc, Woonsocket, RI, USA). For spectral data acquisition, a key point to note is that the grapes and cherry fruit were only measured with the ASI setup, while the pear fruit were measured with Felix handheld spectrometer, USA, and a high-end laboratory spectrometer called Lab spec, ASD, USA. Two extra spectrometers

Table 1
A summary of fruit and reference properties analysed to demonstrate the potential of the ASI setup.

Fruit (Variety)	Total samples	Property
Black grapes	100	Soluble solids
Green grapes	100	Soluble solids
Cherry fruit	100	Soluble solids
Pear	200	Soluble solids

were used to benchmark the performance of the ASI setup with the commercially available spectrometers currently used for non-destructive analysis.

2.4. Chemometric data modelling to validate the functioning of the setup

In this study, two main chemometric data modelling tasks were performed. The first modelling was performed to show the functioning of the ASI system, and the second modelling was performed to benchmark the performance of the ASI system with respect to the commercially available spectrometer systems. For the first part of the analysis, data for grapes and cherry fruit were used, while for the second part, data from the pear fruit were used. More description of the specific analysis is as follows.

2.4.1. Analysis for testing functionality of the ASI setup

To test the functionalities of the ASI setup, three partial least-square regression (PLSR) [30,31] models were developed on 60% of the data and were tested on the remaining 40% of the data. The three models were for black grapes, green grapes, and cherry fruit, respectively. The PLSR models were developed and tested on the mean spectra extracted by manually drawing the region of interest on the top surface of the fruit. Please note that the mean spectra were only taken from the central part of fruit with a square of size 10×10 pixels. Such an extraction was performed to avoid the spectra from the curved surface of fruit which may suffer from physical light scattering effects. The spectra were partitioned as model training (60%) and independent testing (40%) using the Kennard-Stone algorithm [32]. The optimal number of latent variables were selected using a 5-fold cross-validation procedure. Prior to data modelling, the mean spectra were reduced to the near-infrared (NIR) spectral range of 700−1000 nm as SSC have the most correlation with the NIR spectral range. Furthermore, the spectra were smoothened [33] and normalised with the standard normal variate (SNV) [34] to compensate for any inhomogeneity in illumination [22]. The spectral pre-processing was performed using the in-house software in MATLAB 2018b (Natick, MA, USA). The PLSR was performed with the 'plsregress' function available in the Statistics and Machine Learning Toolbox in MATLAB 2018b (Natick, MA, USA). Once the PLSR models were calibrated and tested, the prediction maps for SSC were generated by applying the model on each pixel of the spectral image. The performance of individual models was evaluated as the root mean squared error of prediction (RMSEP) on the corresponding independent test sets.

2.4.2. Analysis for benchmarking the performance of the ASI setup

To benchmark the performance of the ASI setup with respect to the commercially available spectrometers, three different PLSR models were developed for predicting SSC in pear fruit. The three models were related to data collected with ASI setup, Felix hand-held setup and ASD Lab spec spectrometer, respectively. Since all three spectral sensors recorded the spectral data in different spectral ranges, to have a fair comparison, all spectral data were reduced to a common spectral range of 700−1000 nm.

Furthermore, the spectra were partitioned as model training (60%) and independent testing (40%) using the Kennard-Stone (KS) algorithm [32]. Like previous analysis, the optimal number of latent variables were selected using a 5-fold cross-validation procedure. As before, the spectra were smoothened [33] and normalised with the standard normal variate (SNV) [34]. The model performances were evaluated as the root mean squared error of prediction (RMSEP) on the independent test set. To compare the performance of the three spectrometers, a 1-way analysis of variance (ANOVA) was performed on the predictions over the independent test set from all three spectrometers. All analysis was carried out in MAT-LAB 2018b (Natick, MA, USA).

3. Results and discussion

3.1. Validation analysis of the performance of the setup

The validation analysis to show the performance of the ASI setup was performed using the black grapes, green grapes, and cherry fruit. The reflectance spectra (Fig. 2A−C), SNV normalised spectra (Fig. 2D−F) and corresponding reference SSC (%) (Fig. 2G−I) for the three types of fruit are shown in Fig. 2. The spectral profiles show typical fresh fruit spectra with the low reflection in the visible region i.e., <670 nm and high reflectance in the NIR range >670 nm. The low reflection in the visible region is due to the presence of fruit pigments in the fruit skin, while the high reflection in the NIR regression is due to the presence of high moisture in the fresh fruit. Furthermore, there was also a rapid transition from visible to NIR and can be related to the red-edge reflection related to the photosynthetic activity of the fresh fruit. For black grapes (Fig. 2A) and cherry (Fig. 2C), the reflection in the visible region was lower, compared to the green grapes (Fig. 2B). The green grapes have a higher reflection in the visible region due to the presence of the chlorophyll pigment in the grape skin imparting green colour to the grapes. In the spectra presented for low, mid, and high SSC fruit, differences in the reflectance and normalised reflectance intensities can be noted, such differences are indicative of the presence of variability related to the differences in SSC in fruit samples. Furthermore, the SSC range of different fruit suggests that black grapes have the widest range of SSC, 18−30%, while the range of green grapes and cherry fruit was between 8 and 20%. Such a high SSC range for black grapes shows that it had sweeter fruit compared to green grapes and cherry.

The performance of the PLSR model calibrated and independently tested for green grapes, black grapes and cherry are shown in Fig. 3. The RMSEP for all three fruits were lower than 0.8%, which is typically in the prediction range of NIR spectroscopy [18,19]. For grapes, the performance of the spectral setup was better than cherry, however, this could be due to the difficulty in extracting the juice from the cherry fruit compared to grapes, as the spectral measurements were performed in a standardised way for all three fruits. The main benefit of the ASI setup is its capability to provide spatial distribution maps of the physicochemical properties. As an example, the spatial distribution maps of the SSC in the cherry fruit are shown in Fig. 4. In Fig. 4, the visualisation illustrates that the cherry fruit has wide variability in the SSC content. A key point to note is that on the borders the effect of fruit shadow is dominant in some fruit, and a reason for it was the blue background plate used for holding fruit. To avoid this problem, in future use, black high-absorbing material plates should be used.

3.2. Comparative analysis of the performance of the setup with market popular point spectrometers

In the earlier section, a demonstration of the functioning of the
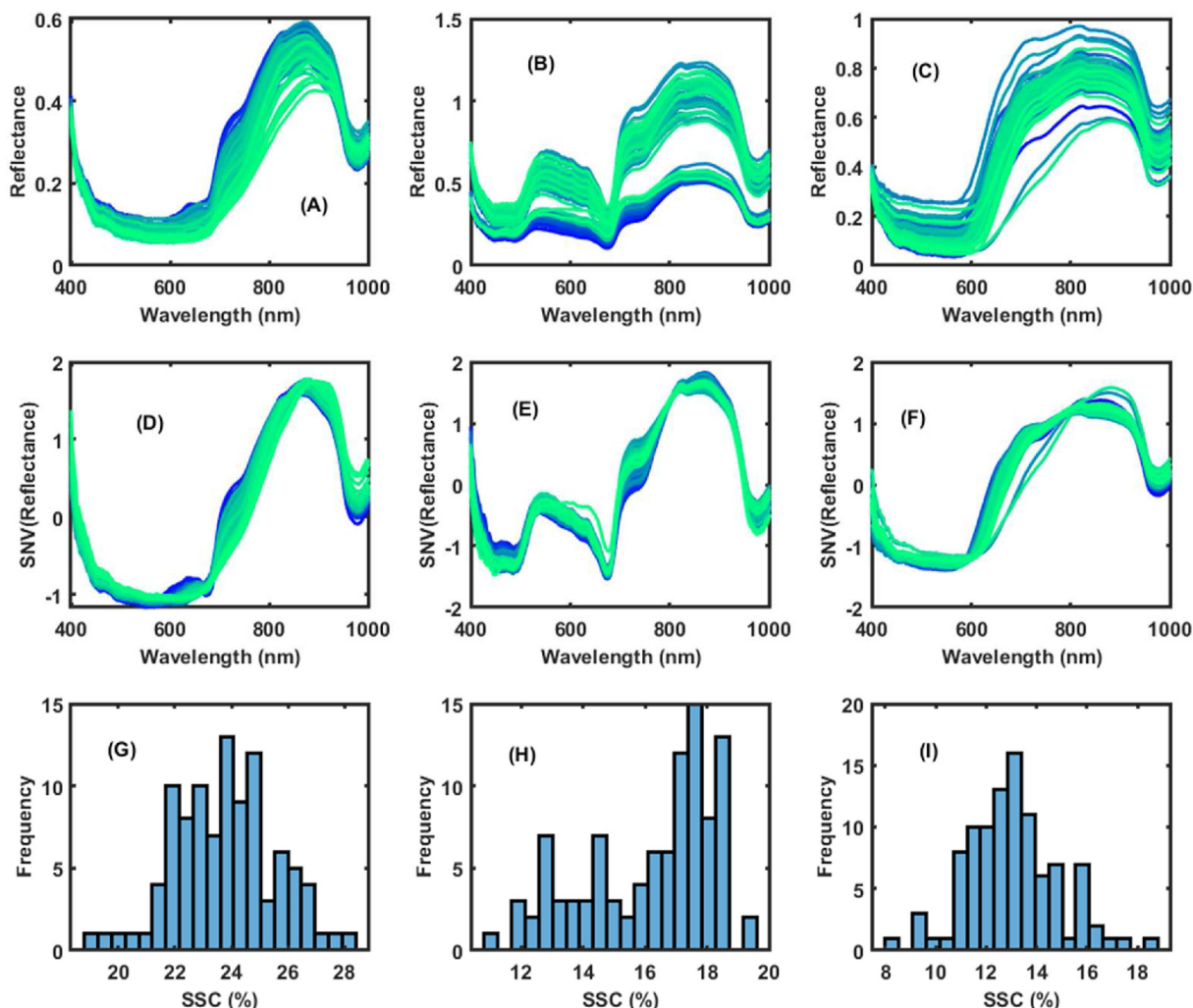
Fig. 2. Spectra corresponding to various levels of soluble solids content and soluble solids distributions for grapes and cherry fruit. Reflectance spectra (blue to green transition indicates low to high SSC values) for (A) black grapes, (B) green grapes, and (C) cherry. Standard normal variate normalised spectra for black grapes (D), green grapes (E), and cherry (F). Soluble solids content distribution in black grapes(G), green grapes (H), and cherry (I). (For interpretation of the references to colour in this figure legend, the reader is referred to the Web version of this article.)

ASI setup using the grapes and cherry fruit was showed. In this section, the performance of the ASI setup in comparison with two popular point spectrometers commonly used for fresh fruit analysis was showed. The mean spectra of pear fruit from different spectrometers are shown in Fig. 5. Since different spectrometers has different spectral ranges, in Fig. 5A the mean spectra in the complete spectral ranges are shown, while in Fig. 5B, the mean spectra in the common spectral range of 400−1000 nm are shown. Spectra from all three spectrometers in the spectral range of 400−1000 nm showed a similar reflectance pattern i.e., low reflection in the visible part and high reflection in the NIR part. The spectra of the Felix spectrometer showed higher reflection in the NIR part. An apparent reason for such a high reflection of the Felix spectrometer is unknown but the only assumed reason could be the different mode of measurement compared to ASI setup and ASD Lab spec. Unlike ASI setup and ASD Lab spec which acquire data in diffuse reflection, the Felix instrument acquires data in interaction mode. The performance of the PLSR calibration performed with spectral data from different sensors on the pear data set is shown in Table 2. In terms of RMSEP, the performances of all the three spectrometers were similar ranging from 0.40 to 0.52% which is in the typical range of SSC prediction in pear with NIR spectroscopy [35,36].

Although the point spectrometer showed a slightly lower RMSEP compared to the ASI setup, the differences between the prediction (Fig. 6) of different spectrometers were insignificant as the 1-way ANOVA analysis (Table 3) reached a F-score of 0.88.

4. Conclusions

This study involved developing a new all-in-one spectral imaging (ASI) system for standardised image acquisition and real-time model deployment. The functioning of the setup was showed using a case of soluble solids content prediction in a range of fresh fruits. Furthermore, the performance of the developed system was benchmarked with the commercial point spectrometer systems currently available in the market. The result showed that ASI system allowed a precise prediction of soluble solids content over three types of fresh fruit, grapes, cherry, and pear. Moreover, the comparison with commercial spectrometers showed that the ASI setup achieved similar performance and there were insignificant differences between the prediction of ASI setup and the commercial spectrometers widely used for NIR analysis. Although in this study the demonstration case involved a prediction of soluble solids content, ASI can be used to analyse any type of samples
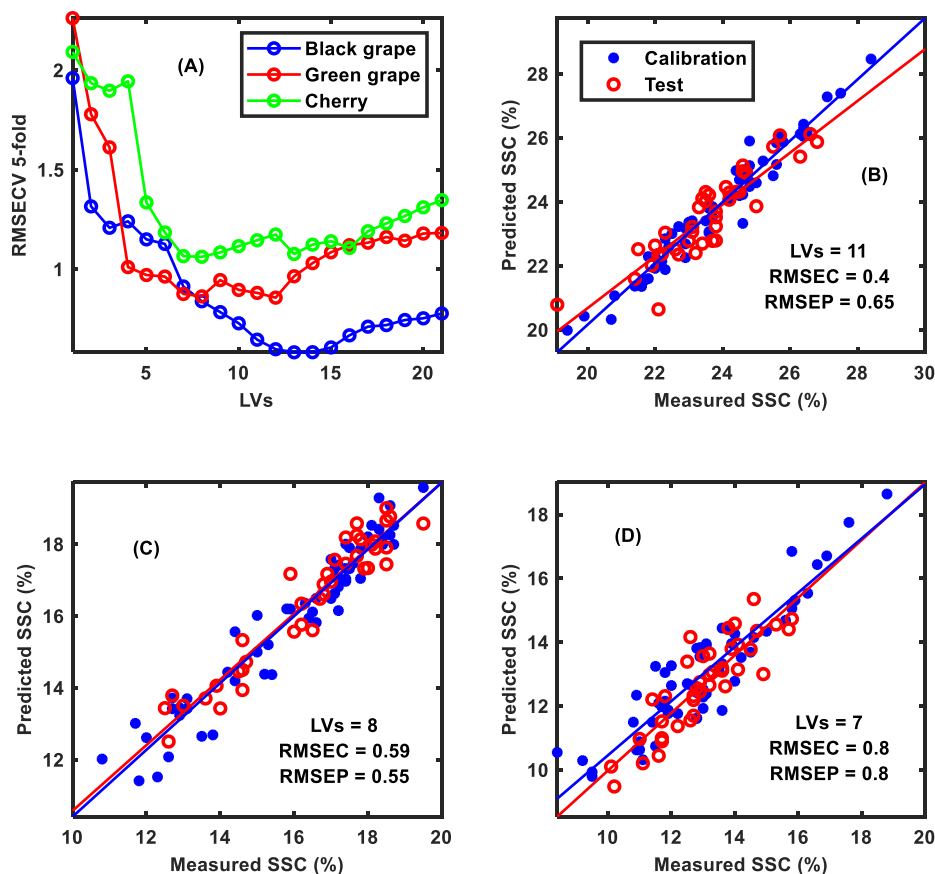
Fig. 3. Performance of PLSR calibration for soluble solids content prediction. (A) cross-validation plot, (B) prediction plot for black grapes, (C) prediction plot for green grapes, and (D) prediction plot for cherry. (For interpretation of the references to colour in this figure legend, the reader is referred to the Web version of this article.)
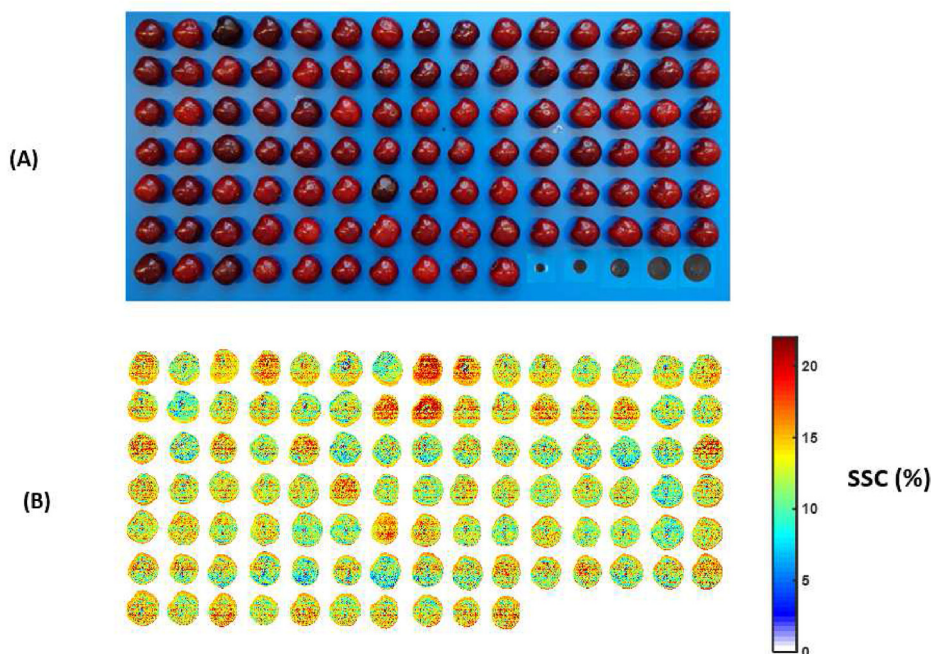
Fig. 4. Spatial distribution map for soluble solids content (SSC) predicted in cherry fruit. (A) RGB images, and (B) soluble solids content distribution maps.

where NIR spectroscopy is of interest. A key benefit of ASI setup compared to the market available point spectrometers is that it allows exploring spatially distributed properties due to the rich spatial information captured by the SI. A special attention was given
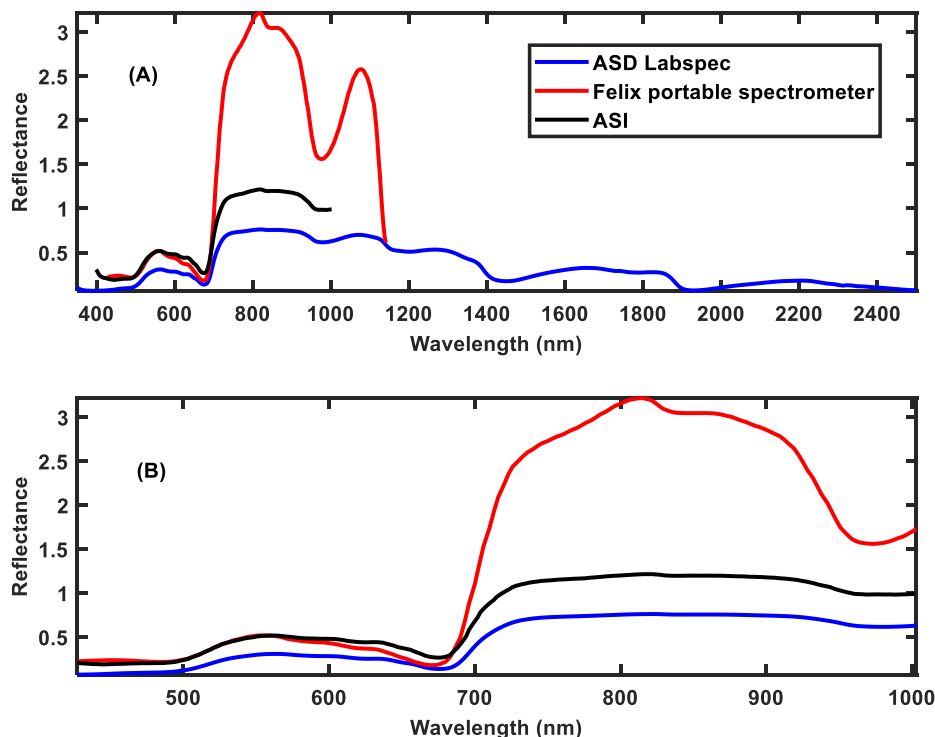
Fig. 5. Mean pear fruit spectra from three different spectroscopy setups. (A) spectra in the full spectral range of each sensor, and (B) spectra chopped to 400−1000 nm for each spectroscopy setup to keep the analysis comparable.

Table 2
A summary of root mean squared error of prediction for Felix, ASD Lab Spec, and ASI setup.

Sensor	Root mean squared error of prediction for SSC (%)
ASD Lab spec	0.48
Felix handheld	0.40
AI−In-One spectral imaging	0.52
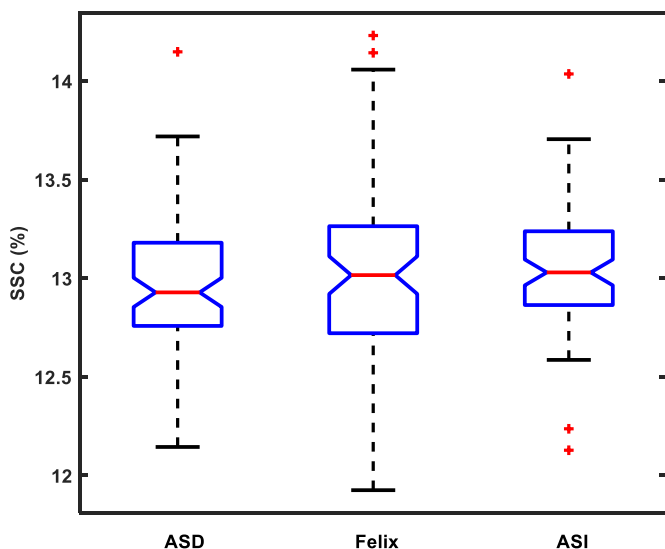
Fig. 6. Whisker box plot to explain the predictions on the same test set by different spectral sensors.

Table 3
1-way analysis of variance results for prediction from three different sensors.

Source	SS	df	MS	F	Prob > F
Groups	0.24	2	0.12	0.88	0.42
Error	33.31	237	0.14		
Total	33.55	239			

spectral data and models usually acquired during laboratory experiments with the help of embedded computing. The ASI setup will contribute to the wider usage of spectral sensing where models and data can be shared between different users of spectroscopy.

CRediT authorship contribution statement

Puneet Mishra: Conceptualization, Methodology, Software, Formal analysis, Writing − original draft. **Menno Sytsma:** Conceptualization, Methodology. **Aneesh Chauhan:** Conceptualization, Methodology, Software, Formal analysis, Writing − original draft, Funding acquisition. **Gerrit Polder:** Conceptualization, Methodology, Software, Formal analysis, Writing − original draft. **Erik Pekkeriet:** Conceptualization, Supervision, Project administration, Funding acquisition.

to usability of the tool so that it is accessible to expert and non-expert users alike. The new ASI setup promotes the reuse of

Declaration of competing interest

The authors declare that they have no known competing financial interests or personal relationships that could have appeared to influence the work reported in this paper.

Acknowledgments

References

[1] R. Joshi, S. Lohumi, R. Joshi, M.S. Kim, J. Qin, I. Baek, B.-K. Cho, Raman spectral analysis for non-invasive detection of external and internal parameters of fake eggs, Sensor. Actuator. B Chem. 303 (2020) 127243.

[2] L.M. Kandpal, S. Lohumi, M.S. Kim, J.-S. Kang, B.-K. Cho, Near-infrared hyperspectral imaging system coupled with multivariate methods to predict viability and vigor in muskmelon seeds, Sensor. Actuator. B Chem. 229 (2016) 534−544.

[3] A. Ambrose, S. Lohumi, W.-H. Lee, B.K. Cho, Comparative nondestructive measurement of corn seed viability using Fourier transform near-infrared (FT-NIR) and Raman spectroscopy, Sensor. Actuator. B Chem. 224 (2016) 500−506.

[4] E. Park, S. Lohumi, B.-K. Cho, Line-scan imaging analysis for rapid viability evaluation of white-fertilized-egg embryos, Sensor. Actuator. B Chem. 281 (2019) 204−211.

[5] C. Pasquini, Near infrared spectroscopy: a mature analytical technique with new perspectives − a review, Anal. Chim. Acta 1026 (2018) 8−36.

[6] R.F. Lu, R. Van Beers, W. Saeys, C.Y. Li, H.Y. Cen, Measurement of optical properties of fruits and vegetables: a review, Postharvest Biol. Technol. 159 (2020).

[7] W. Saeys, N.N. Do Trong, R. Van Beers, B.M. Nicolai, Multivariate calibration of spectroscopic sensors for postharvest quality evaluation: a review, Postharvest Biol. Technol. (2019) 158.

[8] M. Li, Z.Q. Qian, B.W. Shi, J. Medlicott, A. East, Evaluating the performance of a consumer scale SCiO (TM) molecular sensor to predict quality of horticultural products, Postharvest Biol. Technol. 145 (2018) 183−192.

[9] R.A. Crocombe, Portable spectroscopy, Appl. Spectrosc. 72 (2018) 1701−1751.

[10] C.A.T. dos Santos, M. Lopo, R.N.M.J. Pascoa, J.A. Lopes, A review on the applications of portable near-infrared spectrometers in the agro-food industry, Appl. Spectrosc. 67 (2013) 1215−1233.

[11] P. Mishra, R. Nikzad-Langerodi, F. Marini, J.M. Roger, A. Biancolillo, D.N. Rutledge, S. Lohumi, Are standard sample measurements still needed to transfer multivariate calibration models between near-infrared spectrometers? The answer is not always, Trac. Trends Anal. Chem. (2021) 116331.

[12] P. Mishra, Ct-Gui: A graphical user interface to perform calibration transfer for multivariate calibrations, Chemometr. Intell. Lab. Syst. 214 (2021) 104338.

[13] P. Mishra, A. Biancolillo, J.M. Roger, F. Marini, D.N. Rutledge, New data preprocessing trends based on ensemble of multiple preprocessing techniques, Trac. Trends Anal. Chem. (2020) 116045.

[14] P. Mishra, D. Passos, A synergistic use of chemometrics and deep learning improved the predictive performance of near-infrared spectroscopy models for dry matter prediction in mango fruit, Chemometr. Intell. Lab. Syst. (2021) 104287.

[15] P. Mishra, D. Passos, Realizing transfer learning for updating deep learning models of spectral data to be used in a new scenario, Chemometr. Intell. Lab. Syst. (2021) 104283.

[16] P. Mishra, J.-M. Roger, D.N. Rutledge, A short note on achieving similar performance to deep learning with practical chemometrics, Chemometr. Intell. Lab. Syst. 214 (2021) 104336.

[17] P. Mishra, D.N. Rutledge, J.-M. Roger, K. Wali, H.A. Khan, Chemometric preprocessing can negatively affect the performance of near-infrared spectroscopy models for fruit quality prediction, Talanta (2021) 122303.

[18] K.B. Walsh, V.A. McGlone, D.H. Han, The uses of near infra-red spectroscopy in postharvest decision support: a review, Postharvest Biol. Technol. 163 (2020) 111139.

[19] K.B. Walsh, J. Blasco, M. Zude-Sasse, X. Sun, Visible-NIR 'point' spectroscopy in postharvest fruit and vegetable assessment: the science behind three decades of commercial use, Postharvest Biol. Technol. 168 (2020) 111246.

[20] J.M. Amigo, I. Martí, A. Gowen, F. Marini, Chapter 9 - Hyperspectral Imaging and Chemometrics: A Perfect Combination for the Analysis of Food Structure, Composition and Quality, Data Handling in Science and Technology, Elsevier, 2013, pp. 343−370.

[21] Y. Lu, W. Saeys, M. Kim, Y. Peng, R. Lu, Hyperspectral imaging technology for quality and safety evaluation of horticultural products: a review and celebration of the past 20-year progress, Postharvest Biol. Technol. 170 (2020) 111318.

[22] P. Mishra, S. Lohumi, H. Ahmad Khan, A. Nordon, Close-range hyperspectral imaging of whole plants for digital phenotyping: recent applications and illumination correction approaches, Comput. Electron. Agric. 178 (2020) 105780.

[23] M.M. Ali, N.A. Bachik, N.A. Muhadi, T.N.T. Yusof, C. Gomes, Non-destructive techniques of detecting plant diseases: a review, Physiol. Mol. Plant Pathol. 108 (2019).

[24] A.A. Gowen, C. O'Sullivan, C.P. O'Donnell, Terahertz time domain spectroscopy and imaging: emerging techniques for food process monitoring and quality control, Trends Food Sci. Technol. 25 (2012) 40−46.

[25] A.A. Gowen, C.P. O'Donnell, P.J. Cullen, G. Downey, J.M. Frias, Hyperspectral imaging − an emerging process analytical tool for food quality and safety control, Trends Food Sci. Technol. 18 (2007) 590−598.

[26] S. Lohumi, S. Lee, B.-K. Cho, Optimal variable selection for Fourier transform infrared spectroscopic analysis of starch-adulterated garlic powder, Sensor. Actuator. B Chem. 216 (2015) 622−628.

[27] L.M. Kandpal, B.-K. Cho, J. Tewari, N. Gopinathan, Raman spectral imaging technique for API detection in pharmaceutical microtablets, Sensor. Actuator. B Chem. 260 (2018) 213−222.

[28] C. Wakholi, L.M. Kandpal, H. Lee, H. Bae, E. Park, M.S. Kim, C. Mo, W.-H. Lee, B.-K. Cho, Rapid assessment of corn seed viability using short wave infrared line-scan hyperspectral imaging and chemometrics, Sensor. Actuator. B Chem. 255 (2018) 498−507.

[29] N. Mobaraki, J.M. Amigo, HYPER-Tools. A graphical user-friendly interface for hyperspectral image analysis, Chemometr. Intell. Lab. Syst. 172 (2018) 174−187.

[30] S. Wold, M. Sjostrom, L. Eriksson, PLS-regression: a basic tool of chemometrics, Chemometr. Intell. Lab. Syst. 58 (2001) 109−130.

[31] S. Wold, PLS Modeling with Latent Variables in Two or More Dimensions, 1987.

[32] R.W. Kennard, L.A. Stone, Computer aided design of experiments, Technometrics 11 (1969) 137−148.

[33] A. Savitzky, M.J.E. Golay, Smoothing and differentiation of data by simplified least squares procedures, Anal. Chem. 36 (1964) 1627−1639.

[34] R.J. Barnes, M.S. Dhanoa, S.J. Lister, Standard normal variate transformation and de-trending of near-infrared diffuse reflectance spectra, Appl. Spectrosc. 43 (1989) 772−777.

[35] P. Mishra, F. Marini, B. Brouwer, J.M. Roger, A. Biancolillo, E. Woltering, E.H.-v. Echtelt, Sequential fusion of information from two portable spectrometers for improved prediction of moisture and soluble solids content in pear fruit, Talanta 223 (2021) 121733.

[36] P. Mishra, E. Woltering, B. Brouwer, E. Hogeveen-van Echtelt, Improving moisture and soluble solids content prediction in pear fruit using near-infrared spectroscopy with variable selection and model updating approach, Postharvest Biol. Technol. 171 (2021) 111348.